

Ab initio thermal conductivity of thermoelectric Mg_3Sb_2 : evidence for dominant extrinsic effects

Maria Barbara Maccioni, Roberta Farris, and Vincenzo Fiorentini
*Department of Physics at University of Cagliari, and CNR-IOM,
UOS Cagliari, Cittadella Universitaria, I-09042 Monserrato (CA), Italy*
(Dated: December 4, 2018)

The lattice thermal conductivity of the candidate thermoelectric material Mg_3Sb_2 is studied from first principles, with the inclusion of anharmonic, isotope, and boundary scattering processes, and via an accurate solution of the Boltzmann equation. We find that the anomalously low observed conductivity is due to grain-boundary scattering of phonons, whereas the purely anharmonic conductivity is an order of magnitude larger. Mass disorder due to alloying and off-stoichiometry is also found to contribute significantly to its decrease. Combining ab initio values vs sample size with measured grain-size distributions, we obtain an estimate of κ vs T in nano-polycrystalline material in good agreement with typical experiments, and compute the ZT figure of merit in the various cases.

Thermoelectricity is emerging as a viable energy source for a number of applications that recycle thermal waste, and materials with a high thermoelectric figure of merit

$$\text{ZT} = \frac{\sigma S^2}{\kappa} T,$$

where σ and κ are the electrical and thermal conductivities, S the Seebeck coefficient, and T the temperature, are currently in growing demand. Recently, Mg_3Sb_2 has been studied fairly extensively [1–7] as a prototype of a family of so-called Zintl phases that have emerged as interesting candidates. The main focus has been at first on electronic properties, as the Seebeck coefficient in this family is somewhat larger than usual due to its multi-valley conduction band manifold. Equally significant for ZT, however, is the thermal conductivity of Mg_3Sb_2 and its doped relatives, which is unusually low for a crystalline material, namely $\kappa \simeq 1.5 \text{ W K}^{-1}\text{m}^{-1}$ around room T (with considerable experimental scatter). The thermal conductivity $\kappa = \kappa_\ell + \kappa_e$ is the sum of lattice and electronic contributions; κ_e is often modest (of order $1 \text{ W K}^{-1}\text{m}^{-1}$ [8]) at the typical doping used in this material and generally in thermoelectric applications, and it can be phased out by reducing the doping density. Thus, the interesting anomaly must reside in the lattice contribution κ_ℓ being unusually small.

At present, there is no theoretical estimate of κ based on direct state-of-the-art calculations. In particular, it is not obvious that intrinsic vibrational properties be responsible for the low κ . In this paper we provide an ab initio assessment of lattice thermal conductivity in Mg_3Sb_2 , including third-order anharmonic scattering processes, isotopic scattering, and Casimir finite-size boundary scattering. We find that the low thermal conductivity is due to microstructure size effects, i.e. to grain boundary scattering of phonons due to polycrystallinity. Boundary scattering reduces the thermal conductivity due to anharmonic scattering by as much as an order of magnitude for relevant crystallite sizes; signifi-

cant isotopic scattering (peculiar to the isotopic composition of Mg and Sb) and structural anisotropy (due to the hexagonal structure) further contribute to reducing κ_ℓ . After exploring the effects of different ingredients, we estimate an average κ_ℓ vs T in polycrystalline Mg_3Sb_2 with nanosized grains by combining ab initio values vs sample size with measured grain-size distributions. We finally use the calculated κ_ℓ in a calculation of the figure of merit ZT. In all cases, results seem in fair to satisfactory agreement with typical experiments.

We use the Quantum Espresso suite [9] to optimize the structure of Mg_3Sb_2 and obtain the phonon spectrum, and the D3Q-Thermal2 codes [10, 11] for the anharmonic force constants, thermal conductivity, and q -dependent linewidths, including Casimir and isotopic-disorder scattering. We use generalized-gradient (GGA) density-functional theory (DFT) [12] for electron-electron interaction, and Hartwigsen-Goedecker-Hutter [13] norm-conserving pseudopotentials for electron-ion interaction. The plane-wave cut-off is set at 50 Ry, and the k -points grids are $8 \times 8 \times 8$ for both structure optimization and phonon dynamical-matrix calculations, $4 \times 4 \times 4$ for the third-order force constants, and $10 \times 10 \times 10$ for the thermal conductivity. For the thermal conductivity calculation, the "exact" iterative conjugate-gradient solution method of Ref.[11] (Sect.III) is used, with δ functions mimicked by Gaussians with a width of 5 cm^{-1} . Tests on grids, cutoff, and widths, suggest that the lattice thermal conductivity value is stable to within about 5%.

The calculated lattice thermal conductivity κ_ℓ in a vibrationally-harmonic crystal is infinite. Phonon-phonon interactions due to anharmonicity cause it to become finite, with a roughly $\sim 1/T$ behavior above the Debye temperature, and still diverging as temperature goes to zero. If the finite size of the crystal is accounted for [15–17], κ_ℓ becomes finite at zero T and generally decreases at all T's. In addition, if different isotopes of the constituents exist, ionic mass disorder further reduces κ_ℓ .

Figure 1 presents the computed lattice thermal con-

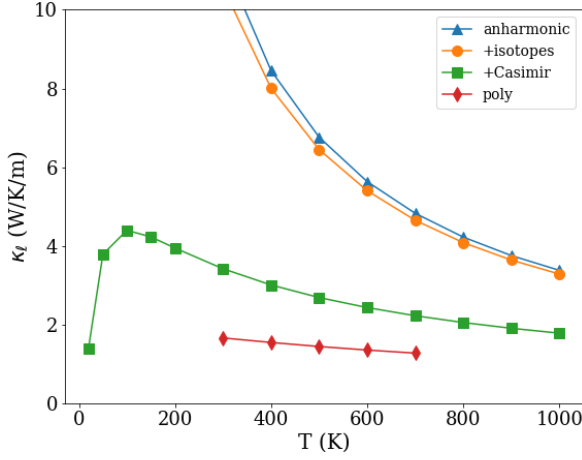


FIG. 1. Temperature dependence of κ_ℓ in Mg_3Sb_2 . From top: anharmonic; anharmonic and isotopes; anharmonic, isotopes and Casimir ($L=50$ nm). The lowest curve (diamonds) is the average conductivity over an experimental grain-size distribution in Mg_3Sb_2 polycrystals (see text and Figure 2).

ductivity κ_ℓ in several different variants. In all cases (see below for the lowest curve), we plot the inverse average of the tensor components (which are $\kappa_\ell^{xx}=\kappa_\ell^{yy}\simeq 1.1$ κ_ℓ^{zz} ; there is no off-diagonal component in zero magnetic field). The anharmonic scattering processes result in a κ_ℓ (upper curve in the Figure) of over 10 at room T, which is typical of crystals, but nearly a factor 10 larger than most experimental reports. Isotopic disorder scattering reduces κ_ℓ (second curve from top), as expected from the significant naturally-occurring isotopic diversity of Mg and Sb [14], but the effect is not nearly enough to cure the discrepancy. We then include Casimir boundary scattering. We choose isotropic shape and, for demonstration purposes, a size of $L=50$ nm. The result is the third curve from top in Figure 1, which shows that finite-size scattering at this length decreases κ_ℓ by a factor of about 3 at room temperature, to somewhere around a factor 2-3 the experimental value. In all calculations including Casimir scattering we have assumed the correction factor [11] for shape and roughness [15–17] to be $F=1$, which we deem appropriate to isotropic grains with rough surfaces and separated by sizable disordered regions, such as those found in this material [7]. We checked, at room temperature, that the often-used [11, 18] value $F=0.5$ would in fact reinforce our conclusions, reducing $\bar{\kappa}_\ell$ by a further 15-20%.

Now we consider that the average value of κ_ℓ in polycrystalline samples will be determined by the grain size distribution and shape. We thus investigate the size dependence of κ_ℓ , and set up a simple estimate based on actual grain distributions [6]. Figure 2 reports the size-dependent $\kappa_\ell(L)$ (the usual inverse average of the components) at 300 K, along with the normalized grain-size distribution n_L , imported from Figure 3a of Ref.6 (the

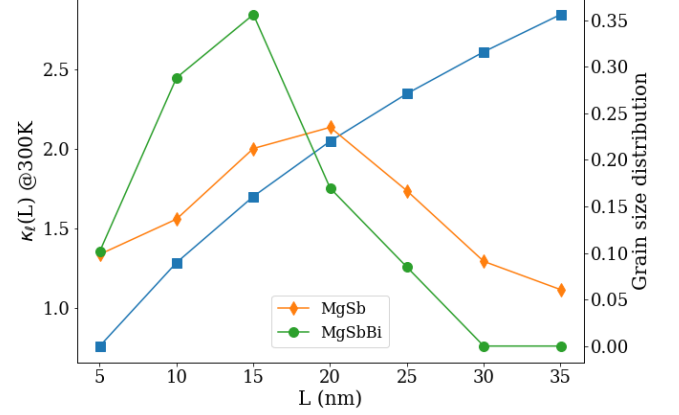


FIG. 2. $\kappa_\ell(L)$ of Mg_3Sb_2 at 300 K (squares, left vertical axis), and the distributions (from Ref.[6], normalized; right vertical axis) of grain sizes vs L in Mg_3Sb_2 and $\text{Mg}_3\text{Sb}_{1.8}\text{Bi}_{0.2}$.

same distribution for a $\text{Mg}_3\text{Sb}_{1.8}\text{Bi}_{0.2}$ alloy from Figure 3d of Ref.6 is also reported: see below for discussion). Evidently, the grain distribution is quite localized over small values (about 20 nm on average) and becomes negligible at larger values. To average over the grains, we assume that thermal transport will occur “in series” across randomly-oriented grains of size L with abundance given by the normalized distribution n_L , so that

$$\bar{\kappa}_\ell = 1 / \left[\sum_L \frac{n_L}{\kappa_\ell(L)} \right].$$

The result at 300 K is $\bar{\kappa}_\ell \simeq 1.65$, which is in line with typical experiments. (We note that the specifics of averaging are not crucial; one could argue instead that $\bar{\kappa}_\ell = \kappa_\ell(L_{\text{ave}})$ for an average grain size, say at the peak of the distribution, and still get essentially the same value.)

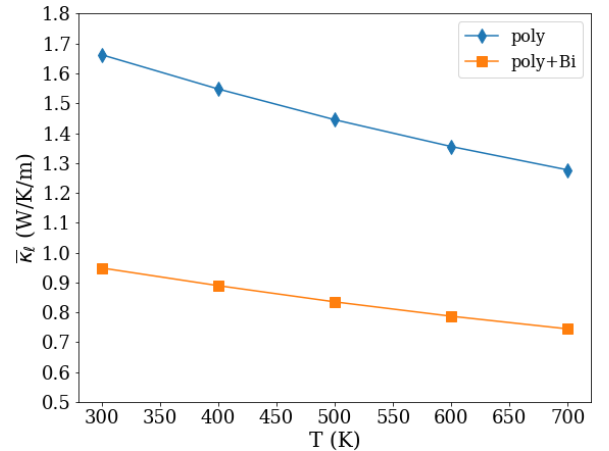


FIG. 3. $\bar{\kappa}_\ell$ in poly- Mg_3Sb_2 (diamonds, same as Figure 1) and $\text{Mg}_3\text{Sb}_{1.8}\text{Bi}_{0.2}$ (see text).

Repeating the L -dependent calculations at other temperatures, we finally obtain the lowest curve (diamonds) in Figure 1, which is indeed as close to the experimental data (e.g. Figure 5c of Ref.[6]) as the intrinsic variability of grain sizes and shapes will reasonably allow. This indicates that polycrystallinity is the likely cause of the low thermal conductivity, and is therefore an essential ingredient of thermoelectric efficiency in Mg_3Sb_2 .

In Figure 3 we assess qualitatively the behavior of $\bar{\kappa}_\ell$ in a low-concentration $\text{Mg}_3\text{Sb}_{1.8}\text{Bi}_{0.2}$ alloy. We calculate $\kappa_\ell(L)$ with Bi acting as a fictitious Sb isotope of 10% relative abundance in the isotope scattering term; in addition, we import the size distribution of the nanocrystalline alloy with the same composition from Figure 3d of Ref.[7] (also displayed in Figure 2 above) and calculate the average. The two effects reduce $\bar{\kappa}_\ell$ by roughly equal amounts; both the temperature trend and the change in conductivity values are, within the limits of such simple model estimate, in fair agreement with experiments [1]. The predicted conductivity would be probably further lowered if the actual phonon spectrum and anharmonic scattering in a Bi-containing alloy were included, due to the softer Bi-related modes. This calculation suggests that, while polycrystallinity remains the major factor, mass disorder contributes significantly to the reduction of κ_ℓ (see also below).

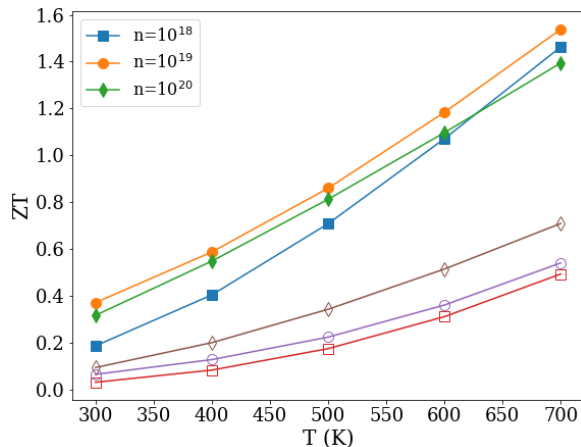


FIG. 4. ZT vs T in a Mg_3Sb_2 for three n -type doping levels (in cm^{-3}) using the perfect crystal (empty symbols) and polycrystal (filled symbols) lattice thermal conductivity.

The figure of merit ZT of Mg_3Sb_2 is reported in Figure 4, for both the perfect crystal and the polycrystal, for three n -type doping levels. Clearly, the poly and crystal situations are quite different, very possibly setting apart thermoelectrically useful vs useless material. ZT vs doping density has a maximum near 10^{19} cm^{-3} for the poly case, while it increases monotonically for the crystal case, due to the different ratio of the electrical and lattice components of κ , and the different T -behavior of the two κ_ℓ 's (due to the very definition of ZT). Overall, ZT for our

model of a n -doped Mg_3Sb_2 polycrystal is essentially in the experimental ballpark (see Figure 1a, Ref.[1]).

All electronic transport coefficients used to produce Figure 4 are obtained with the Bloch-Boltzmann transport code BoltzTrap [19] including phonon and impurity scattering via an energy- and temperature-dependent relaxation time [8, 20], which was tested in previous applications [21]. The electronic structure is again obtained within GGA-DFT, using the projector augmented wave method as implemented in the VASP code [22]. Full details are reported elsewhere [8]. We use the total thermal conductivity $\kappa = \kappa_\ell + \kappa_e$, since the electronic thermal conductivity κ_e is not generally negligible. The lattice part is either the crystal value, or the grain-average $\bar{\kappa}_\ell$ discussed above. For all the electronic transport coefficients we use the crystal values, since we found that, within the model of Ref.[7], the effects of grain boundaries on electrical quantities are marginal (of order 0.5-1%) at our typical doping, with ZT even increasing slightly in the poly case due to a compensation of the decrease in σ and κ_e , and the increase in S .

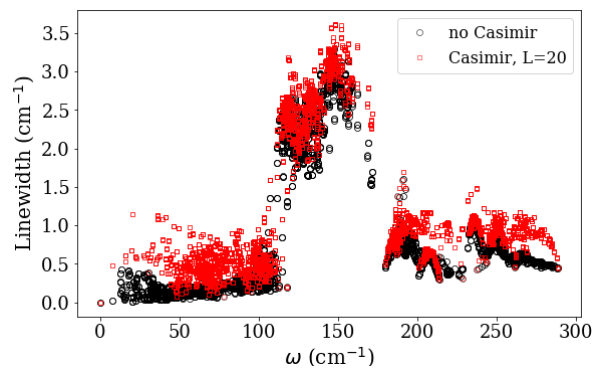


FIG. 5. Phonon linewidths vs energy with and without Casimir scattering, $L=20$ nm, $T=300$ K.

We close with a brief discussion of the phonon-phonon and finite-size phonon scattering linewidths. Figure 5 shows linewidths vs energy for the entire spectrum. The central region between 100 and 150 cm^{-1} clearly dominates the linewidths; as pointed out in Ref.23, this spectral region is the only one involving significantly the octahedrally-coordinated Mg cation, which has much longer bonds to Sb (as well as an anomalous effective dynamical Born charge of 3.6 vs about 2 of the other two, tetrahedrally-coordinated, Mg's).

Casimir scattering mainly affects lower-energy modes, as borne out by Figure 6, depicting the phonon dispersion (inclusive of the quasiparticle interaction shift) with superimposed linewidths for the lower part of the spectrum at $T=300$ K. Both anharmonic and Casimir scattering are especially significant along the Γ -A-L-M- Γ circuit, with the A and M points being the most significant region of scattering overall. This agrees with the identification of Ref.[23] (see in particular Figure 5 thereof)

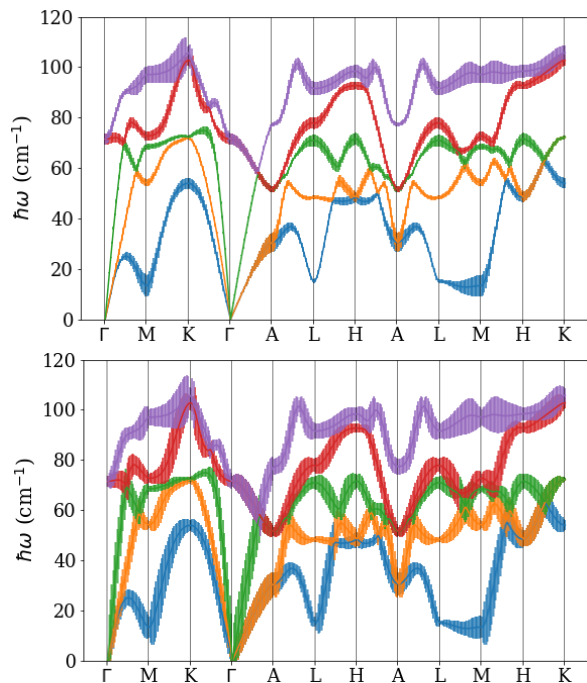


FIG. 6. Linewidths for low-energy phonons (including anharmonic shifts) at 300 K. Top figure: anharmonic and natural-isotope scattering, infinite size; bottom panel: same, plus Casimir scattering, $L=20$ nm.

of the shearing transverse-acoustic mode as a significant locus of anharmonicity and scattering in this material.

We now discuss comparison with experiments in general and with other recent theoretical estimates of κ_ℓ , referring for brevity to room T values. Other than the present one, there appears to be no calculation using DFPT for phonons and anharmonicity, and the full iterative Boltzmann equation solution, with inclusion of phonon depopulation and repopulation. Two papers [25, 26] use harmonic and anharmonic force constants obtained via a fit to frozen-phonon distortions in real-space supercells to build the relaxation time for use in the Boltzmann equation. Ref.[25] reports $\kappa_\ell \simeq 1.5$ W/(K m) computed from the Boltzmann equation in the single-mode approximation. All the force constants are obtained in supercells equivalent to a $4 \times 4 \times 4$ k-grid, very close to ours in terms of anharmonicity. Next, Ref.[26] also reports $\kappa_\ell \simeq 1.5$ W/(K m) at room T, obtained again from the Boltzmann equation in an unspecified approximation; harmonic and anharmonic force constants are calculated, respectively, in $4 \times 4 \times 2$ and $3 \times 3 \times 3$ supercells, slightly smaller than in the other case, but probably not critical, judging from the tests provided.

The difference with our result may stem from a combination of factors (some of which inter-related and not easily disentangled) in these technically complex calculations. First, the phonon group velocities are calculated as finite differences on k-grids (unspecified in the papers),

based on force constants obtained on relatively coarse equivalent grids ($4 \times 4 \times 2$ or $4 \times 4 \times 4$). By contrast, our method directly evaluates group velocities from the interpolated dynamical matrix (see Ref.[11], Sec.IV), which is obtained originally on a finer $8 \times 8 \times 6$ grid. Second, in the Boltzmann equation solution, convergence in k-point sampling and δ -widths may be imperfect (it is unspecified in both papers) and, third, the single-mode approximation [25] may artificially reduce κ_ℓ (this is a known, occasionally large, effect [11]). By contrast, we use the full iterative solution of Ref.[11] and carefully checked convergence in grid and widths. (From our data, we estimate a κ_ℓ reduction of order 30% from single-mode solution and grid halving, but have no way of checking the effect of finite-differences differentiation; we also caution that our single-mode solution is a modified one.)

We also mention Ref.[24] which reports $\kappa_\ell \simeq 2.5$ W/(K m), obtained via an expression involving average Grüneisen parameters and sound velocities. Although a low thermal conductivity is indeed plausibly related to large Grüneisen parameters (see also Ref.[23]), this remains a simple phenomenological model. On a different note, the estimated ZT of over 2.5 in the same paper is a significant overestimate, mainly due to the neglect of electronic thermal conductivity, as well as to the constant-relaxation-time approximation [8].

As to experimental results in general, many papers report low thermal conductivities around 1 to 1.5 W/(K m) or so in Mg_3Sb_2 -based polycrystals and alloys (including, for example, Ref.[25]), and are in general agreement with our proposed explanation. For single crystals, Ref.[27] reports $\kappa_\ell \simeq 1.5$ W/(K m) at room T in nominally pure and perfect single crystals, as well as in alloys. This low single crystal value contrasts significantly with our prediction. As to this specific work, it is unclear whether this value is representative of macroscopic single-crystals, as κ shows a typical finite-size downturn at low T (similar to that of Ref.[3] in sintered poly material, see also below); also, it is puzzling that polycrystals and single crystals would have essentially the same κ_ℓ .

More generally, and aside from Ref.[27] specifically, a proper comparison is predicated on experiments being done on disorder-free single crystals. However, single crystals are apparently hard to come by (and may in fact be uninteresting technologically), intentional alloying is ubiquitous, and general defectivity and off-stoichiometry are considerable. Differences in preparation (sintering, etc.), impurity content, texture, composition etc. cause significant fluctuations in the data; for example Ref. [3] gives (extrapolating in Fig.6c therein) around 6 W/(K m) in μm -scale polycrystals (with $L=1 \mu\text{m}$ we get about 7 W/(K m)); Ref.[5] reports 2.5-3 W/(K m) in hot-pressed pellets, dropping to about 1.5 W/(K m) in alloyed material. All of this suggests that Mg_3Sb_2 and related materials come in a wide spectrum of crystallite sizes and/or disorder states.

In this context, a serious possibility that emerges is that microscopic disorder in the supposedly single-crystal samples contributes significantly to a lowered κ_ℓ . Indeed, thermal conductivity can be efficiently suppressed by random mass disorder (an extreme example is $\kappa_\ell=120$ W/K/m in pure Si dropping by a factor 40 upon 20% Ge random admixture [28]); since this scattering term is very similar to isotope disorder, we calculated κ_ℓ without boundary scattering (i.e. in a periodic crystal) with an fictitious composition $\text{Mg}_{2.99}\text{Sb}_{1.5}\text{Bi}_{0.5}$ (similar to experiments in Ref.[25] plus Mg off-stoichiometry) mimicking strong mass disorder: at 300 K we get $\kappa_\ell \simeq 1.6$ W/(K m), which is in the experimental ballpark (this estimate of course does not include changes in the phonon spectrum or anharmonic couplings). So we can tentatively conclude that κ_ℓ can also be suppressed by large mass disorder alone (as well as by polycrystallinity or combinations of the two). In the light of all these uncertainties, a definitive comparison with experiments for crystals should await measurements in unambiguously large, pure, and well-ordered single crystals.

In summary, we proposed that the lattice thermal conductivity (and hence, by and large, the total conductivity in typical thermoelectric applications) of Mg_3Sb_2 is not anomalously small for intrinsic reasons, but rather because of Casimir grain-boundary scattering. While the bulk thermal conductivity is around 10 W/(K m) at room T, it drops to about 1.5 W/(K m) or less for a typical experimental distribution of grain sizes. Strong microscopic mass disorder, e.g. in alloys, also contributes significantly to the suppression of κ_ℓ . The final prediction for κ_ℓ , as well as the figure of merit ZT, in a nano-polycrystal is in good agreement with experiment.

Work supported in part by UniCA, Fondazione di Sardegna, Regione Sardegna via Progetto biennale di ateneo 2016 *Multiphysics approach to thermoelectricity*, and CINECA-ISCRA grants. We thank Lorenzo Paulatto for sharing his developer version of D3Q/Thermal2, and for useful discussions.

Note added in proof: After acceptance, we estimated from model scattering rates [8] that in lightly doped Mg_3Sb_2 crystals the large electron-polar phonon coupling (Frölich constant $\simeq 0.6$ vs. Pauling ionicity 13%) may decrease the thermal conductivity by as much as 20-30%.

[1] J. Zhang, L. Song, S. Hindborg Pedersen, H. Yin, L. T. Hung, and B. Brummerstedt Iversen, *Nature Comm.* **8** 13901 (2017).
 [2] A. Bhardwaj, N. S. Chauhan, S. Goel, V. Singh, J. J. Pulikkotil, T. D. Senguttuvan, and D. K. Misra, *Phys. Chem. Chem. Phys.* **18**, 6191 (2016).
 [3] C. L. Condon, S. M. Kauzlarich, F. Gascoin, and G. J.

Snyder, *J. Sol. St. Chem.* **179**, 2252 (2006).
 [4] A. Bhardwaj, A. Rajput, A. K. Shukla, J. J. Pulikkotil, A. K. Srivastava, A. Dhar, Govind Gupta, S. Auluck, D. K. Misra and R. C. Budhani, *RSC Advances* **3**, 8504 (2013).
 [5] F. Ahmadpoura, T. Kolodiazhnyi, and Y. Mozharivskyja, *J. Sol. St. Chem.* **180**, 2420 (2007).
 [6] A. Bhardwaj, N. S. Chauhan, and D. K. Misra, *J. Mater. Chem. A* **3**, 10777 (2015).
 [7] J. J. Kuo, S. Dongmin Kang, K. Imasato, H. Tamaki, S. Ohno, T. Kanno, and G. J. Snyder, *Energy Environ. Sci.* **11**, 429 (2018).
 [8] R. Farris, M. B. Maccioni, A. Filippetti, and V. Fiorentini, *J. Phys.: Condens. Matter*, in print (2018). See also <https://arxiv.org/abs/1807.07513>.
 [9] P. Giannozzi *et al.*, *J. Phys.: Condens. Matter* **21**, 395502 (2009); *ibid.*, **29**, 465901 (2017).
 [10] L. Paulatto, F. Mauri, and M. Lazzeri, *Phys. Rev. B* **87**, 214303 (2013).
 [11] G. Fugallo, M. Lazzeri, L. Paulatto, and F. Mauri, *Phys. Rev. B* **88**, 045430 (2013).
 [12] J. P. Perdew, K. Burke, and M. Ernzerhof, *Phys. Rev. Lett.* **77**, 3865 (1996).
 [13] C. Hartwigsen, S. Goedecker, and J. Hutter, *Phys. Rev. B* **58**, 3641 (1998).
 [14] J. S. Coursey, D. J. Schwab, J. J. Tsai, and R. A. Dragoset, *Atomic Weights and Isotopic Compositions* (National Institute of Standards and Technology, Gaithersburg, MD, 2015).
 [15] O. Bourgeois, D. Tainoff, A. Tavakoli, Y. Liu, C. Blanc, M. Boukhari, A. Barski, and E. Hadji, *C. R. Physique* **17**, 1154 (2016).
 [16] R. Berman, F. E. Simon and J. M. Ziman, *Proc. Royal Soc. London A* **220**, 171 (1953); R. Berman, E. L. Foster and J. M. Ziman, *Proc. Royal Soc. London A* **231**, 130 (1955); J. M. Ziman, *Electrons and phonons* (Clarendon Press, Oxford, 1960).
 [17] H. B. G. Casimir, *Physica* **5**, 495 (1938).
 [18] A. Sparavigna, *Phys. Rev. B* **65**, 064305 (2002).
 [19] G. K. H. Madsen and D. J. Singh, *Comput. Phys. Commun.* **175**, 67 (2006).
 [20] M. Balkanski and R. F. Wallis, *Semiconductor Physics and Applications* (Oxford University Press, New York, 2000); B. K. Ridley, *Quantum Processes in Semiconductors* (Clarendon Press, Oxford, 1988).
 [21] P. Delugas *et al.*, *Phys. Rev. B* **88**, 045310 (2013); *ibid.*, 115304; *ibid.* **91**, 115315 (2015).
 [22] G. Kresse and J. Furthmüller, *Phys. Rev. B* **54**, 11169 (1996); G. Kresse and D. Joubert, *ibid.* **59**, 1758 (1999).
 [23] W. Peng, G. Petretto, G.-M. Rignanese, G. Hautier, and A. Zevalkink, *Joule* (2018), <https://doi.org/10.1016/j.joule.2018.06.014>
 [24] J. Li, S. Zheng, T. Fang, L. Yue, S. Zhang, and G. Lu, *Phys. Chem. Chem. Phys.* **20**, 7686 (2018).
 [25] H. Tamaki, H. K. Sato, and T. Kanno, *Adv. Mater.* **28**, 10182 (2016).
 [26] J. Zhang *et al.*, <https://arxiv.org/abs/1807.00599v1>.
 [27] S. H. Kim *et al.*, *J. Mater. Chem.A* **2**, 12311 (2014).
 [28] J. Garg, N. Bonini, B. Kozinsky, and N. Marzari, *Phys. Rev. Lett.* **106**, 045901 (2011)